JOURNAL OF THERMOPHYSICS AND HEAT TRANSFER
Vol. 16, No. 4, October–December 2002

Computation of Nonequilibrium High-Temperature Axisymmetric Boundary-Layer Flows

P. F. Barbante* and G. Degrez†
von Kármán Institute for Fluid Dynamics, 1640 Rhode Saint Genèse, Belgium
and
G. S. R. Sarma‡
Deutsches Zentrum für Luft und Raumfahrt, 37073 Göttingen, Germany

Efficient and accurate Hermitian-type multipoint finite difference methods are used to develop a general boundary-layer code for analyzing reacting flows around bodies of revolution. The main motivation is to build a reliable code that can be used for the investigation of the influence of different physico-chemical models for transport properties, chemical kinetics, and finite rate wall catalysis on practically relevant quantities like heat flux and skin friction at the body surface. Special care has been devoted to the correct modeling of diffusion fluxes, an aspect that is often neglected in literature. The exact Stefan–Maxwell equations are used to model the diffusion fluxes and are solved with an efficient iterative technique. Finite rate catalysis is an important aspect of thermal protection system (TPS) materials studies, for which a boundary-layer code is a very useful tool because it allows the computation of the heat flux at a cost that is a fraction of a Navier–Stokes approach. Wall catalyticity effects are taken into account by means of a model that allows one to express a suitable set of wall reactions with the associated reaction-rate probabilities. Computations performed on a variety of problems and the results shown here on some typical test cases indicate the ability and reliability of the code to cope with a wide range of nonequilibrium conditions, making it a potentially useful tool for physico-chemical and TPS material studies.

Nomenclature

c_i	=	mass fraction of species i, ρ_i/ρ
$\mathcal{D}_{ij}$	=	binary diffusion coefficient between species i and j, m^2/s
E_{amb}	=	ambipolar electric field, V/m
h	=	mixture enthalpy, J/kg
h_i	=	enthalpy of species i, J/kg
J_i	=	mass diffusion flux of species i, kg/(m^2 s)
$J_i^{\downarrow}$	=	mass flux of species i incident to the wall, kg/(m^2 s)
k	=	Boltzmann constant
k_{fr}, k_{br}	=	forward and backward reaction rates; see Eq. (6)
M	=	mixture molar mass, kg/mol
M_i	=	molar mass of species i, kg/mol
m_i	=	mass of particle i, kg
p	=	pressure, Pa
q	=	heat flux, W/m^2
q_i	=	charge of species i per unit mass, C/kg
R_{nose}	=	body nose radius, m
r	=	distance from axis in axisymmetric configuration, m
T	=	mixture temperature, K
u, v	=	tangential and normal velocity components, m/s
V	=	velocity, m/s
$\dot{w}_i$	=	mass production rate of species i, kg/(m^3 s)
x, y	=	Cartesian coordinates, m
x_i	=	mole fraction of species i
γ	=	wall recombination probability
η	=	transformed y coordinate
λ	=	mixture thermal conductivity, W/(m K)
μ	=	mixture viscosity, m^2/s
ν'_{ir}, ν''_{ir}	=	forward and backward stoichiometric coefficients
ξ	=	transformed x coordinate
ρ	=	mixture density, kg/m^3
ρ_i	=	density of species i, kg/m^3

Subscripts

b	=	backward reaction
f	=	forward reaction
stag	=	stagnation point
w	=	wall surface
δ	=	boundary-layer outer edge
∞	=	freestream

Presented as Paper 2000-2437 at the AIAA 34th Thermophysics Conference, Denver, CO, 19–22 June 2000; received 3 December 2001; revision received 16 April 2002; accepted for publication 18 April 2002.

*Ph.D. Candidate, Aeronautics and Aerospace Department, Chaussée de Waterloo 72; currently Postdoctoral Fellow, Politecnico di Milano, Dipartimento di Matematica, Piazza Leonardo da Vinci 32, 20133 Milan, Italy; barbante@mate.polimi.it.

†Adjunct Professor, Aeronautics and Aerospace Department, Chaussée de Waterloo 72; also Professor, Université Libre de Bruxelles, Avenue F. D. Roosevelt 50, 1050 Brussels, Belgium. Senior Member AIAA.

‡Research Scientist, Institute of Aerodynamics and Flow Technology, Bunsenstrasse 10; also Adjunct Professor, von Kármán Institute for Fluid Dynamics, 1640 Rhode Saint Genèse, Belgium. Associate Fellow AIAA.

Introduction

HYPERSONIC aerothermochemistry is important for a wide range of applications toward current and future vehicle designs, their propulsion concepts, and related ground-simulation facilities. Although some big programs such as the National Aerospace Plane (NASP), Hermes, and HOTOL have been shelved, scientific and technological interest has been aroused and is kept alive through other programs like capsule technology (X-38, USA; ARD, ESA; HYFLEX, Japan; SHEN-ZHOU, China), reusable launch vehicles like X-33, X-34 (USA) and ARIANE V (Europe), as well as conceptual studies like Crew Transfer Vehicle (Europe), TAKANIS (France), SÄNGER (Germany). The basic scientific challenge in this context is tackling the complex physico-chemical phenomena that occur in high-temperature flowfields of the relevant configurations. A better understanding and control of these phenomena (than is at present possible) is essential for an efficient and ultimately economical design of the new vehicle concepts envisaged.[1] Although

the formal sets of governing equations and boundary conditions for describing the multicomponent reacting flows can be written down, their application to individual configurations is beset with formidable problems especially as a result of a lack of adequate and reliable phenomenological models and associated data for the complete specification of the problem. Increasingly sophisticated computational power can obviously be applied successfully only when the required inputs into the mathematical models are ensured and qualified.[1,2]

In this paper efficient and accurate Hermitian-type multipoint finite difference methods are used to develop a general boundary-layer code for analyzing reacting flows around bodies of revolution. A motivation for the study from a computational fluid dynamics (CFD) point of view is to compare the relative efficiency and economy of using Euler + boundary-layer calculations vs full Navier–Stokes calculations. From a physical point of view, the motivation is the possibility of investigating the effects, especially on practically relevant quantities such as heat transfer and skin friction at the walls, of different physico-chemical models for transport and reaction kinetics in multispecies flows and finite-rate wall catalysis. Especially in the study of catalytic properties of thermal protection system (TPS) materials, a boundary-layer code is a very useful tool because it allows the computation of the heat transfer (a necessary step for the determination of TPS materials catalyticity) at a cost that is a fraction of a Navier–Stokes one.[3]

Governing Equations and Related Physico-Chemical Models

We make the following assumptions: the flow is axisymmetric or two-dimensional, laminar, and steady; the influence of body forces from external fields is neglected; the boundary-layer assumptions are valid; the fluid is composed of a mixture of N_s chemical species, each one being a thermally perfect gas.

A Cartesian reference system having the x axis lying on and the y axis normal to the body surface is considered. The unknown quantities are the tangential u and normal v components of the velocity vector, the enthalpy h or alternatively the temperature T, and the mass fraction of the different chemical species $c_1 \ldots c_i \ldots c_{N_s}$. The leading quantities u, v, and h are global, mass-averaged quantities for the whole mixture. In the case of ionized mixtures, local charge neutrality and zero electric current are assumed, the latter being justified by the absence of external electromagnetic fields.

The governing equations are as follows.

Continuity:

$$\frac{\partial \rho u r^{\epsilon}}{\partial x} + \frac{\partial \rho v r^{\epsilon}}{\partial y} = 0 \tag{1}$$

Species continuity:

$$\rho\left(u\frac{\partial c_i}{\partial x} + v\frac{\partial c_i}{\partial y}\right) + \frac{\partial J_i}{\partial y} = \dot{w}_i \tag{2}$$

Momentum:

$$\rho\left(u\frac{\partial u}{\partial x} + v\frac{\partial u}{\partial y}\right) = -\frac{\mathrm{d}p_{\delta}}{\mathrm{d}x} + \frac{\partial}{\partial y}\left(\mu\frac{\partial u}{\partial y}\right) \tag{3}$$

Energy (global):

$$\rho\left(u\frac{\partial h}{\partial x} + v\frac{\partial h}{\partial y}\right) = u\frac{\mathrm{d}p_{\delta}}{\mathrm{d}x} + \mu\left(\frac{\partial u}{\partial y}\right)^2 - \frac{\partial q}{\partial y} \tag{4}$$

(The parameter ϵ defines the geometry; for an axisymmetric case $\epsilon = 1$, and for two-dimensional $\epsilon = 0$.) Additional energy equations can be added if thermal nonequilibrium (which we set aside here) is taken into account.

The heat flux can be written as

$$q = -\lambda\frac{\partial T}{\partial y} + \sum_{i=1}^{N} J_i h_i \tag{5}$$

The Dufour effect here and the Soret effect in Eq. (2) are neglected.

According to the law of mass action, the mass production rate is

$$\dot{w}_i = M_i \sum_{r=1}^{NR} (\nu''_{ir} - \nu'_{ir}) \times \left\{ k_{fr} \prod_{j=1}^{NJ} \left(\frac{\rho c_j}{M_j}\right)^{\nu'_{jr}} - k_{br} \prod_{j=1}^{NJ} \left(\frac{\rho c_j}{M_j}\right)^{\nu''_{jr}} \right\} \tag{6}$$

(NR is the total number of reactions that involve species i, and NJ is the number of species involved in each of the NR different reactions.) We remember that the preceding expression is valid only if the NR reactions considered are elementary reactions, that is, reactions that take place in one single step. The forward reaction rates k_{fr} are taken from Arrhenius data fits available in literature.[4,5] The backward reaction rates are computed from k_{fr} and the equilibrium constant K_{cr}: $k_{\mathrm{br}} = k_{\mathrm{fr}}/K_{\mathrm{cr}}$. The equilibrium constant is linked to the Gibbs free energy and is computed from statistical mechanics.[6]

Different levels of approximation can be employed to compute the transport coefficients (that is, viscosity, thermal conductivity, and diffusion coefficients); parameter studies have been carried out in the stagnation point region,[7] and the main conclusion is that realistic values for the heat transfer can be obtained only if at least a mixture rules model (for example, Wilke[8] and Mason and Saxena[9]) is employed for the computation of the transport coefficients. In this work the mixture transport properties are computed with the method of Chapman and Enskog.[6] The thermodynamic properties of chemical species are computed by means of statistical mechanics methods[6]; anharmonicity corrections for the molecular species can be included.

Special care has been devoted to the computation of the diffusion fluxes J_i. In literature the Fick's law approximation $J_i = -\rho D_i \nabla c_i$ is often used. This formula has the advantage of an easy implementation, but violates mass conservation and gives wrong estimates for the wall heat flux.[10,11] In the present work the Stefan–Maxwell equations, which are equivalent to the detailed Chapman–Enskog multicomponent diffusion equations,[12] are used to model the diffusion fluxes:

$$\frac{M}{\rho}\sum_{j=1}^{N_s}\left(\frac{x_i J_j}{M_j \mathcal{D}_{ij}} - \frac{x_j J_i}{M_i \mathcal{D}_{ij}}\right) = \frac{\partial x_i}{\partial y} - \frac{q_i \rho_i}{p} E_{\mathrm{amb}} \qquad i = 1, \ldots, N_s \tag{7}$$

Pressure and thermal diffusion are neglected, but the influence of the electric field is retained in case of ionized mixtures. The latter is determined by imposing the ambipolar constraint[13] that is, no electric current

$$\sum_{i=1}^{N_s} q_i J_i = 0$$

on the diffusion fluxes J_i, the ambipolar assumption being consistent with the absence of external electromagnetic fields. A method recently proposed by Sutton and Gnoffo[10] is used to solve numerically the Stefan–Maxwell equations. The method has been adapted to handle correctly the ambipolar constraint for ionized mixtures.[11]

Wall catalyticity effects are taken into account as boundary conditions for the species equations. The full range of catalyticity regimes, from noncatalytic wall to fully catalytic wall, can be simulated. As upper extreme a local equilibrium wall boundary condition is available. (The species concentrations at the wall are the ones corresponding to the chemical equilibrium composition at the wall local pressure and temperature.) The catalytic boundary condition is realized imposing $J_{\mathrm{iw}} = \dot{w}_{\mathrm{iw}}$, that is, the diffusion flux toward the wall balances the creation or destruction of species caused by chemical reactions at the wall. The wall reaction rates are expressed in terms of the recombination probability γ (defined as the ratio of the mass flux of ith particles recombining at the surface over the mass flux of

ith particles impinging the surface); if n_r reactions are taking place at the wall, the same number of γ coefficients should be considered. The recombination probabilities are functions of the mixture composition, pressure, and temperature at the surface. The wall reaction rate is defined as

$$\dot{w}_{iw} = J_i^{\downarrow} \sum_{k=1}^{n_r} \nu_{ki} \gamma_k - \sum_{l=1}^{n_r} \sum_{j=1}^{N_s} \mu_{lij} \gamma_l J_j^{\downarrow} \tag{8}$$

The first term in the reaction-rate expression describes the destruction of ith species as a result of wall chemical reactions, the second one the creation of ith species by wall reactions. The matrix ν_k specifies if the ith species is destroyed in the kth reaction; the μ_l matrix specifies if the jth species produces the ith one in the lth reaction. $J_i^{\downarrow}$ is the ith species mass flux incident to the wall, which is given by kinetic theory as $J_i^{\downarrow} = \rho_{iw}\sqrt{(kT_w/2\pi m_i)}$. Scott[14] suggests a modification to properly take into account the first-order perturbation of the Boltzmann distribution in the computation of the incident mass flux $J^{\downarrow}$. Practically this amounts to the definition of a new γ': $\gamma' = 2\gamma/(2-\gamma)$ in Eq. (8). In the present work we use the simple γ definition.

Numerical Solution

The boundary-layer equations are transformed by means of the Lees–Dorodnitsyn coordinate transformation.[15] The new coordinates are defined as

$$\xi(x) = \int_0^x (\rho\mu u)_\delta r^{2\epsilon}\, \mathrm{d}s \tag{9}$$

$$\eta(x, y) = \frac{u_\delta r^\epsilon}{\sqrt{2\xi}} \int_0^y \rho\, \mathrm{d}t \tag{10}$$

The main advantages of this transformation are as follows: the growth of the boundary-layer thickness is incorporated into the transformation itself; axisymmetric flows are treated as equivalent two-dimensional flows.

The boundary-layer equations, also in transformed coordinates, are still parabolic (except the continuity), and this property is exploited in order to split the solution procedure into two distinct steps, one in the direction along the body surface (ξ coordinate) and the other normal to it (η coordinate). In this way the code can compute the solution also in the stagnation point, or at the tip of a sharp cone or a flat plate, where the boundary-layer equations reduce to ordinary differential equations.

The discretization in the ξ direction is done by means of a Lagrangian polynomial of second order in ξ. In a generic streamwise location the unknown quantity w can be written as

$$w(\xi, \eta) = L_m(\xi) w_m(\eta) + L_{m-1}(\xi) w_{m-1}(\eta) + L_{m-2}(\xi) w_{m-2}(\eta) \tag{11}$$

[We assume here that the quantities $w_{m-1}(\eta)$, $w_{m-2}(\eta)$ are known from preceding iterations.] The coefficients $L_{m-i}(\xi)$ are polynomials of second order, with the property that $L_{m-j}(\xi_i) = \delta_{ij}$ (Refs. 11 and 15). In this way it is guaranteed that $w(\xi, \eta) = w_{m-i}(\eta)$ at all of the points ξ_{m-i}. By means of this discretization, the boundary-layer equations are reduced, at the streamwise location ξ_m, to nonlinear ordinary differential equations in η and can be written in the form

$$a \frac{\mathrm{d}^2 w_m}{\mathrm{d}\eta^2} + b \frac{\mathrm{d}w_m}{\mathrm{d}\eta} + c w_m = d \tag{12}$$

with the associated boundary conditions

$$\eta = 0 : f \frac{\mathrm{d}w_m}{\mathrm{d}\eta} + g w_m = h \tag{13}$$

$$\eta = \eta_\delta : w_m = w_\delta \tag{14}$$

Equation (12) is still nonlinear because the coefficients $a, b, \ldots, h$ depend in general on the unknown w_m and its derivatives. The nonlinearity is removed by evaluating the coefficients at the level ξ_m by means of a simple iterative updating procedure. They are first evaluated at the level ξ_{m-1}, and Eq. (12) is solved for the new values of w_m at level ξ_m. The coefficients are then updated by utilizing the new solution, and the computation can be repeated to obtain better prediction at ξ_m. The procedure is stopped when the difference between the solution for w_m at the kth iteration and the one at the $(k-1)$th iteration is less than a fixed tolerance. (We used a tolerance of 10^{-6} here.)

The unknown quantity $w_m(\eta)$ is discretized by means of a Hermitian polynomial of fourth order:

$$w_m(\eta) = \tfrac{1}{2} w_{m,n+1}(t^2 + t) + w_{m,n}(1 - t^2) + \tfrac{1}{2} w_{m,n-1}(t^2 - t) + \alpha t(1 - t^2) + \beta t^2(1 - t^2) \tag{15}$$

[$w_{m,n+1}$, $w_{m,n}$, $w_{m,n-1}$ are the values taken by $w_m(\eta)$ at the locations η_{n+1}, η_n, η_{n-1}, respectively.] The variable t is defined as $t = (\eta - \eta_n)/\Delta\eta$; for $t = 1$, $t = 0$, and $t = -1$, the test function in Eq. (15) equals $w_{m,n+1}$, $w_{m,n}$, and $w_{m,n-1}$, respectively. The two parameters α and β can be chosen freely. The polynomial should be equal to the exact solution of the differential equation in several, in general, arbitrary points. To eliminate the free parameters α and β, we need to equal the polynomial and the exact solution in three collocation points. It is useful and logical to choose the collocation points at the levels $n+1$, n, and $n-1$ in the η direction. Then the parameter t equals 1, 0, and -1. The system of three equations arising from the substitution can be reduced to a unique equation in three unknowns by eliminating the free parameters α and β. The final result is a single equation linking the unknown values of w_m at the points $n+1$, n, $n-1$. The procedure is fourth-order-accurate in step size across the boundary layer, but leads to a tridiagonal algebraic system as second-order methods do.[11,15]

The computational grid for this method is simple: no fixed step size is required in the ξ direction, and so it can be tuned locally. A fixed step size is required in the η direction: usually 100 points are enough (as verified by computations with varying the number of points).

Results

We will show now some results of boundary-layer computations around bodies of revolution. Different catalyticity boundary conditions have been used: noncatalytic, partially catalytic, fully catalytic, and local equilibrium wall.

The first computations to be shown are the ones for the AGARD B test case.[16,17] It is a hyperboloid of revolution with a half-vertex angle θ of 10 deg and a nose radius R_{nose} of 2.54 cm. The radius of the hyperboloid r_b is given as function of the distance s along the surface by the differential equation

$$\frac{\mathrm{d}r_b}{\mathrm{d}s} = \left[1 + \frac{(r_b/R_{\text{nose}})^2}{1 + (r_b/R_{\text{nose}})^2 \tan^2\theta}\right]^{-0.5}$$

The freestream conditions are $T_\infty = 195.46$ K, $p_\infty = 2.04$ Pa, $V_\infty = 6096$ m/s. The computations are carried out for four different mixtures: binary nitrogen (N, N_2), air-5 (O_2, N_2, NO, O, N), air-7 (O_2, N_2, NO, NO^+, O, N, e^-), and air-11 (O_2, N_2, NO, NO^+, O^+, N^+, O_2^+, N_2^+, O, N, e^-). The reaction-rate data set given by Gupta et al.[4] has been used. The outer-edge boundary conditions are taken from Ref. 16, and chemical equilibrium is supposed at the boundary-layer edge. The wall reaction set is $N + N \rightarrow N_2$, $O + O \rightarrow O_2$, $NO^+ + e^- \rightarrow NO$, $O^+ + e^- \rightarrow O$, $N^+ + e^- \rightarrow N$, $O_2^+ + e^- \rightarrow O_2$, $N_2^+ + e^- \rightarrow N_2$; the full set is valid for air-11, the first three reactions are taken into account for air-7, the first two for air-5, and the first one for binary nitrogen.

In Fig. 1 (the subfigure shows a zoom of the nose region) the Stanton number (defined here as $S_t = q_w/0.5\rho_\infty V_\infty^3$) for a fully catalytic wall is shown (that is, the γ for all of the wall reactions are set equal to one); the wall temperature is $T_w = 1000$ K. The nitrogen mixture has the lowest heat flux; this is to be expected because

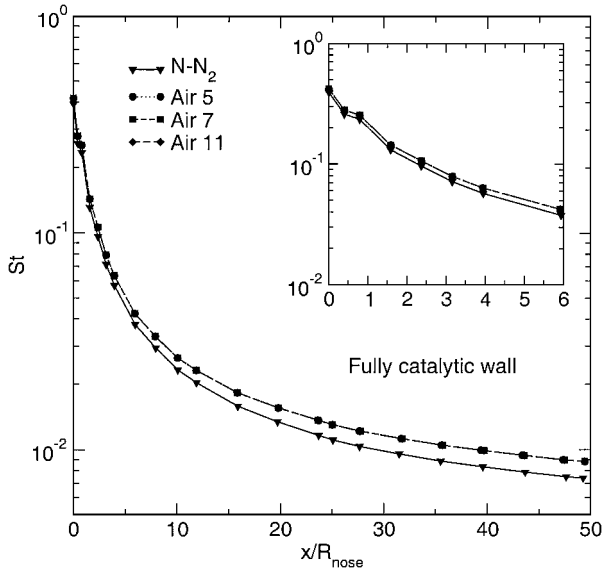

Fig. 1 Stanton number for different air mixtures in AGARD B.

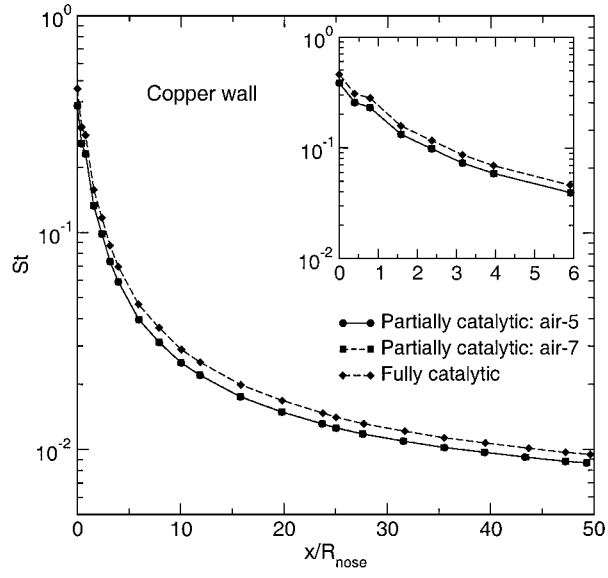

Fig. 3 Stanton number for copper AGARD B sample.

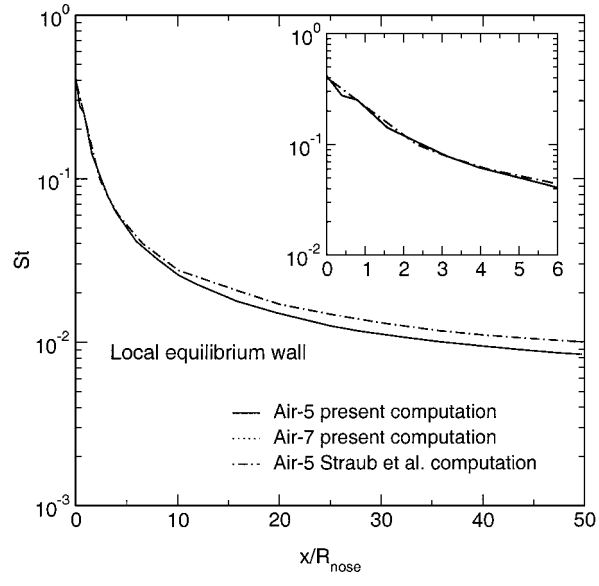

Fig. 2 AGARD B test case: Stanton number comparison with Ref. 16.

oxygen is almost fully dissociated at the boundary-layer outer edge, and its recombination, which happens almost entirely at the wall as a result of catalytic reactions (in effect computations with a noncatalytic wall show only negligible oxygen recombination in the bulk of the boundary layer), raises the heat flux in the air computations. The analysis shows that the catalytic mechanism at the wall can be identified as the main source of the difference in results between air and binary nitrogen because the diffusion mechanism does not distinguish much between oxygen and nitrogen. The heat flux for air-11 and air-7 is slightly higher than for air-5 because of the ions' neutralization at the wall, but, because of the weak ionization degree, this effect is small. The same trend is valid for a local equilibrium wall except that the heat flux is higher, as to be expected.

In Fig. 2, for the sake of comparison, we show the Stanton number for air-5 and air-7 mixtures along with the result taken from Ref. 16; the latter computation has been performed for a chemical equilibrium boundary layer. (As in Fig. 1, the subfigure shows a zoom of the nose region.) We have therefore chosen a local equilibrium wall as boundary condition because it is known that a nonequilibrium boundary layer (or even a frozen boundary layer[18]) with such a boundary condition and a chemical equilibrium boundary layer are giving practically the same value for the heat flux. There is a totally negligible difference between air-5 and air-7 mixture (the same observation being valid for air-11 mixture), and we notice a good agreement between our computations and the one of Ref. 16. The wall heat flux is mainly a function of the difference in enthalpy between the outer edge and the wall. When the wall composition is fixed, as for a local equilibrium wall, the wall enthalpy assumes a value that is independent from what is happening inside the boundary layer. Therefore, differences in physico-chemical modeling play a small role in the determination of the heat-flux final value: this explains the relatively good agreement among the various computations.

To show the ability of the code to cope with different levels of catalyticity and strong temperature gradients in the boundary layer, the AGARD B test case has been recomputed assuming that the hyperboloid is made of copper and the surface temperature is at 150°C. The values of recombination probabilities γ have been taken from literature.[19] Computations have been carried out for air-5 and air-7 mixtures. The wall reaction set is $N + N \rightarrow N_2$, $O + O \rightarrow O_2$, $NO^+ + e^- \rightarrow NO$. As suggested in Ref. 19, we have taken $\gamma_{NN} = 0.29$, $\gamma_{OO} = 0.1$, $\gamma_{NO^+e^-} = 1.0$. The Stanton numbers for the different mixtures are shown in Fig. 3, with the fully catalytic wall for the sake of comparison. (The subfigure shows a zoom of the nose region.) As should be expected, the heat flux for the partially catalytic wall is lower than for the fully catalytic wall; air-7 mixture heat flux is higher than air-5 mixture one, but the difference is very small as a result of the weak ionization level and because of the low wall temperature NO^+ is almost fully recombined before reaching the wall.

We have also performed computations in the stagnation point region of a body that represents the typical geometry of the sample used in the von Kármán Institute Plasmatron wind tunnel[20] to test the catalytic properties of TPS materials. In the specific case it was a cylinder with a circular flat base and a diameter of 1 cm. The outer-edge conditions are given by numerical computations of the flowfield inside the Plasmatron facility,[21] and they are equal to $T_\delta = 4560$ K, $p_\delta = 10{,}161$ Pa, $du_\delta/dx = 11{,}670\ s^{-1}$ (velocity gradient); the chemical composition is the equilibrium one. The computations are performed for air-5 mixture, as at this level of pressure and temperature the ionized species contribution to the heat flux is totally negligible. The wall temperature varies from 300 to 2100 K. The wall reaction set is $N + N \rightarrow N_2$, $O + O \rightarrow O_2$. The value of the catalytic recombination probability γ is taken equal for both reactions and varies from 0 to 1. The reaction-rate data set given by Gupta et al.[4] is used.

In Fig. 4 the heat-flux chart obtained from the computations is shown. The heat-flux curves are parameterized as functions of the catalytic recombination probability γ and are plotted as functions of the wall temperature. The heat flux for a fully frozen flow (that is, no reaction both in the gas and at the wall) is shown in order to assess

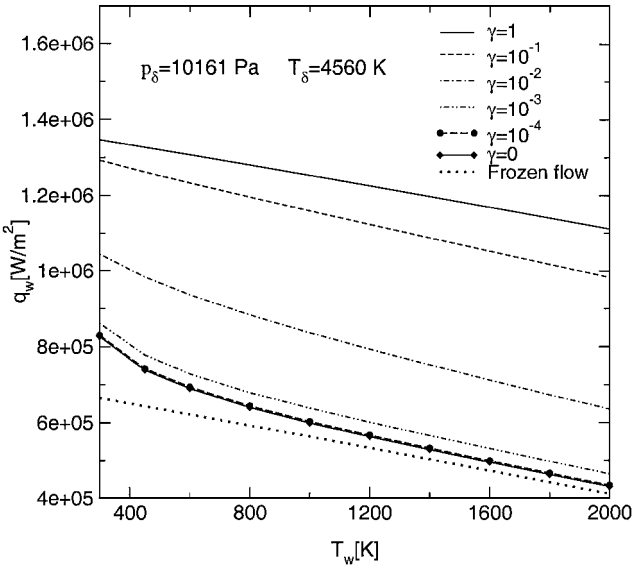

Fig. 4 Heat flux in the stagnation region of a TPS sample.

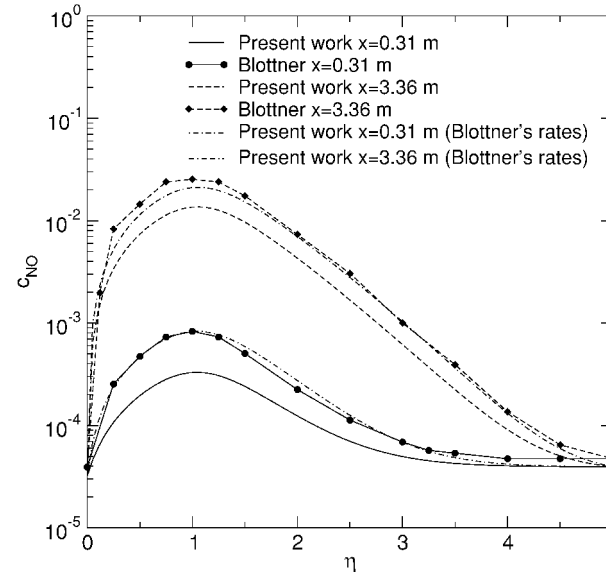

Fig. 6 Nitric oxide mass fraction in the boundary layer.

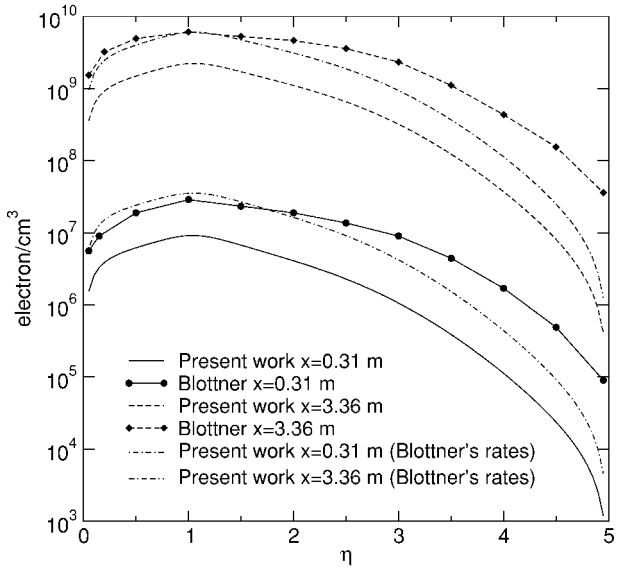

Fig. 5 Electron number density in the boundary layer.

the lower heat-flux limit. It is possible to understand the strong effect of wall catalyticity on the heat flux: at wall temperatures around 1000–1200 K, which are common in reentry situations, the heat flux practically doubles from noncatalytic to fully catalytic conditions. The strong nonlinear dependence of the heat flux from the recombination probability γ might be noticed. When temperature decreases, the difference in heat flux between the frozen case and the noncatalytic one increases. This behavior is caused by a stronger atomic recombination in the gas phase for lower wall temperature. In effect, in the noncatalytic case, because there is no recombination at the wall, the heat-flux difference with respect to the fully frozen flow is caused by the recombination of atomic species inside the bulk of the gas.

Comparisons have been made with the work of Blottner.[22,23] The boundary layer around a 10-deg semivertex angle cone has been computed for the air-7 mixture (the reaction rates being the ones of Gupta et al.[4]). The outer-edge boundary conditions are assumed to be constant along the cone and are equal to $u_\delta = 6581$ m/s, $p_\delta = 25{,}022$ Pa, $T_\delta = 1019$ K (Ref. 22). The outer-edge chemical composition is assumed to be the one corresponding to local chemical equilibrium. The wall temperature is $T_w = 1000$ K, and the wall is a local equilibrium wall. We show the values of electron number density (Fig. 5) and of nitric oxide mass fraction (Fig. 6) at two different streamwise locations; respectively $x = 0.13$ m and 3.36 m. We note that the physical trends are qualitatively the same despite some quantitative differences. The computation was repeated using the same forward and backward reaction rates as in Blottner.[22] Agreement with Blottner results is improved (as shown in Figs. 5 and 6 by the additional curves); residual discrepancies can be explained by differences in the thermodynamic and transport properties and by inherently distinct computational techniques used in the two codes. Blottner numerical method is of lower order accuracy than the Hermitian method used here,[15] the latter being more accurate and efficient for a given number of pivotal points, or alternatively, requiring fewer pivotal points for a given accuracy. This lends more confidence to the better reliability of the results from the present study. Moreover, the kinetic coefficient data and modeling used in the present study are considered more up to date than those of Ref. 22.

Computations were also made for the AGARD A test case [17] (the geometry being the same of the AGARD B test case); it is a good test case to check the ability of the nonequilibrium code to compute a flow near chemical equilibrium. The freestream conditions are $T_\infty = 227$ K, $p_\infty = 1114$ Pa, $V_\infty = 6096$ m/s, which correspond, in the stagnation point, to $T_\delta = 7065$ K and $p_\delta = 605{,}923$ Pa. The outer-edge boundary conditions are taken from Blottner.[23] Air-7 mixture is used in the computations, and the reaction data set of Park[5] is chosen here. Both fully catalytic and noncatalytic walls have been taken into account. The wall reaction set is $N + N \rightarrow N_2$, $O + O \rightarrow O_2$, $NO^+ + e^- \rightarrow NO$; for the fully catalytic case all of the γ have been taken equal to 1; for the noncatalytic case to 0.

In Fig. 7 the species mass fractions at 50 nose radii downstream are shown for a noncatalytic wall. We notice a fairly good agreement for $y/R_{\text{nose}} > 0.1$ for all of the species. Some discrepancies appear for $y/R_{\text{nose}} < 0.1$; higher recombination next to the wall is present in our computations. The fully catalytic wall case (not shown here) has a good agreement for $y/R_{\text{nose}} < 0.1$ too; this is to be expected because the wall chemical composition is imposed by the boundary condition. In Fig. 8 we compare the Stanton number [defined here as $S_t = q_w/\rho_\infty V_\infty (h_{\text{stag}} - h_w)$] along the hyperboloid. We can notice that the heat-flux difference between the noncatalytic and the fully catalytic wall is small; it is clearly an index of the fact that the boundary layer is next to equilibrium. This statement is supported also by the fact that the atomic species (Fig. 7) are appreciably recombining across the boundary layer, even in the case of noncatalytic wall. For the fully catalytic case Blottner computation gives a higher Stanton number in the nose region ($x/R_{\text{nose}} < 1$) and a lower one along the remainder of the body. In the noncatalytic case Blottner gives always a slightly higher heat flux. In both cases the maximum difference does not exceed 8%, a very reasonable value.

We show now in Fig. 9 the Stanton number (defined as in the AGARD B test case) and in Fig. 10 skin-friction {defined

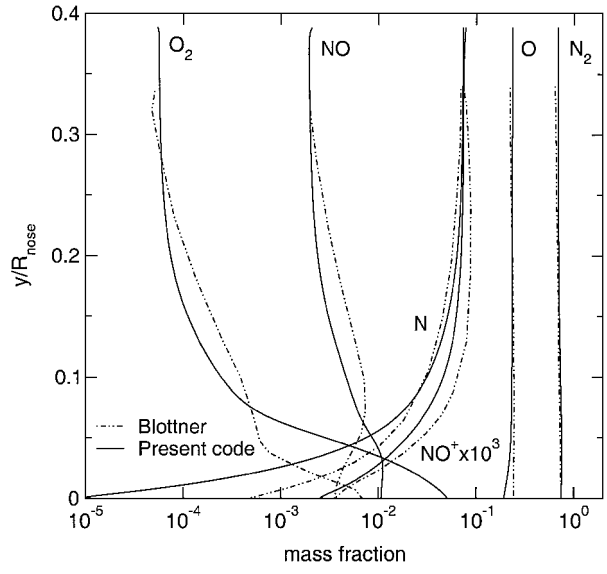

Fig. 7 Species mass fraction for noncatalytic wall at $x/R_{nose} = 50$ for AGARD A test case.

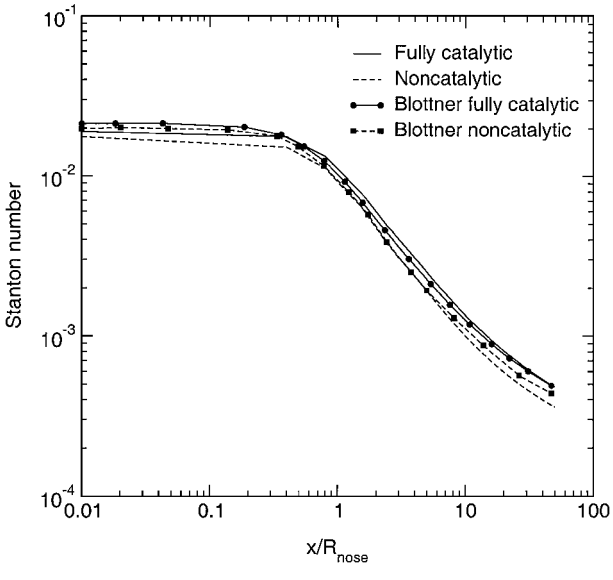

Fig. 8 Stanton number along hyperboloid for AGARD A test case.

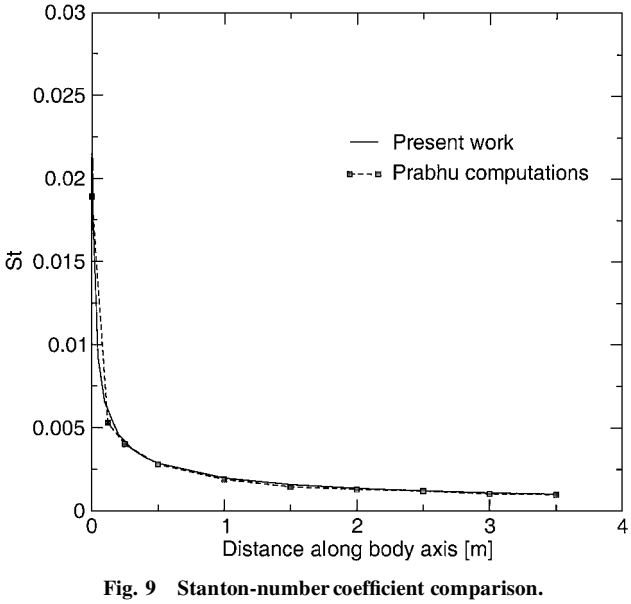

Fig. 9 Stanton-number coefficient comparison.

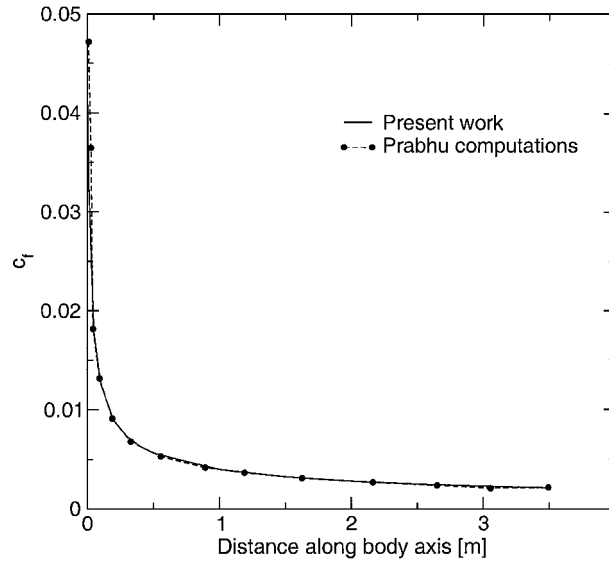

Fig. 10 Skin-friction coefficient comparison.

as $C_f = [\mu(\partial u/\partial y)]_w / 0.5\rho_\infty V_\infty^2\}$ comparisons with the work of Prabhu et al.[24] The computations are carried out for a 10-deg semivertex angle cone at an altitude of 45.72 km with $V_\infty = 8100$ m/s, $p_\infty = 136.7$ Pa, $T_\infty = 266.2$ K. The boundary-layer outer-edge conditions are constant and equal to $u_\delta = 7946$ m/s, $p_\delta = 3750$ Pa, $T_\delta = 1374$ K. The outer-edge chemical composition is taken to be the chemical equilibrium one, although for this pressure and temperature the mixture is practically undissociated. The wall is noncatalytic, and its temperature is $T_w = 1200$ K. The computation has been performed for the air-5 mixture, and the reaction data set of Gupta[4] is chosen here. As can be seen, the agreement between the two codes is very good: a small difference appears only near the cone tip, where the interaction between the inviscid outer flow and the inner boundary layer is not totally negligible.

The Prabhu computations are performed with a parabolized Navier–Stokes code. The good agreement with our boundary-layer results suggests that, in some cases, the "old" approach of combined Euler + boundary-layer computations is still valid. Therefore, the preceding test case has been recomputed following two different strategies: a full Navier–Stokes computation and an Euler + boundary-layer computation. The approach is justified here because the Reynolds number (using as reference length the cone length, which is equal to 3.5 m) is of the order of 3×10^6. The Euler/Navier–Stokes code, also developed by the first author,[11,25] uses the same physico-chemical models as the boundary-layer one. The aim is to compare the relative efficiency and accuracy of an Euler + boundary-layer computation vs a Navier–Stokes one. Both the Euler and the Navier–Stokes computations were performed using second-order-accurate schemes; we recall here that the boundary-layer code is second-order-accurate in the streamwise direction and fourth-order in the direction normal to the wall. The same number of grid points (4489) were used in the Euler and in the Navier–Stokes computations; 100 points were used for the boundary-layer computation. As is usual in the classical Euler + boundary-layer approach, the outer-edge values for the boundary-layer computation have been taken to be the ones at the cone wall for the Euler computation.

In Figs. 11 and 12 the Stanton number and the skin-friction coefficient (defined as in the preceding test case) are shown. (The subfigure shows a zoom of the nose region.) One can notice a certain difference next to the cone tip between the two approaches. The Euler + boundary-layer computation predicts a Stanton number and a skin-friction coefficient appreciably higher than the ones predicted by the Navier–Stokes computation. One reason is that, in the Euler + boundary-layer computation the viscous-inviscid interaction next to the cone tip is neglected. On the other hand, the finite volume grid (for both Euler and Navier–Stokes computations) is not fine enough, in the tip region, to adequately capture all of the fluid

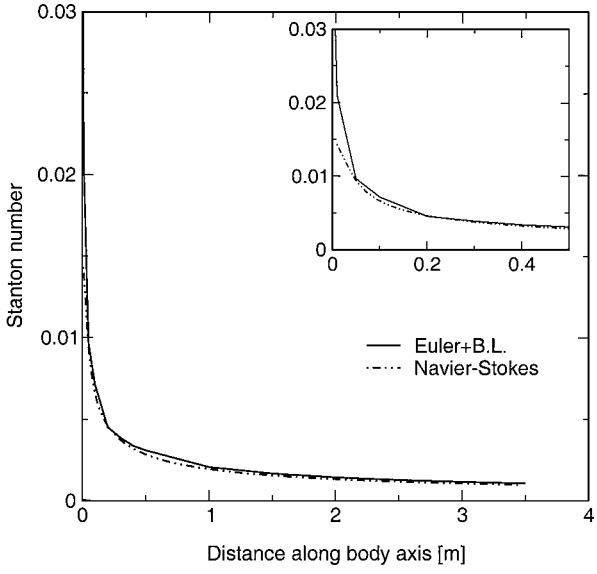

Fig. 11 Stanton-number coefficient comparison for Euler + boundary layer vs Navier–Stokes.

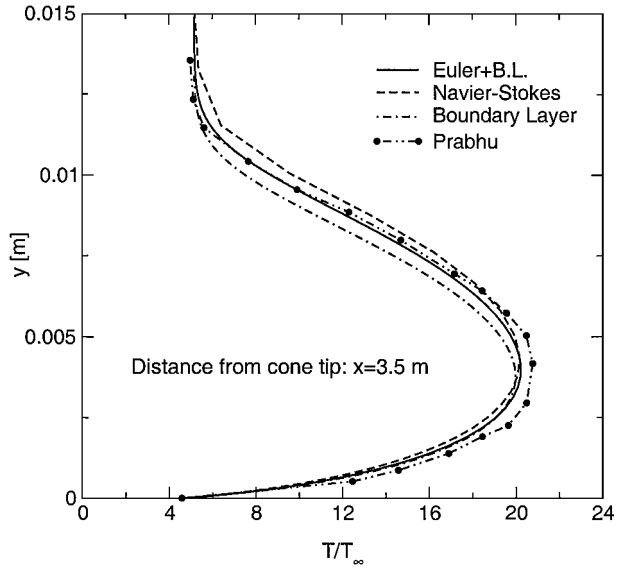

Fig. 13 Nondimensional temperature: comparison among different computations.

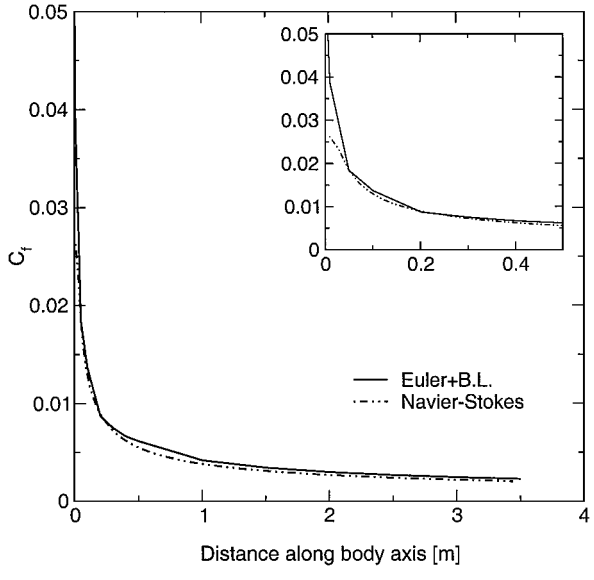

Fig. 12 Skin-friction coefficient comparison for Euler + boundary layer vs Navier–Stokes.

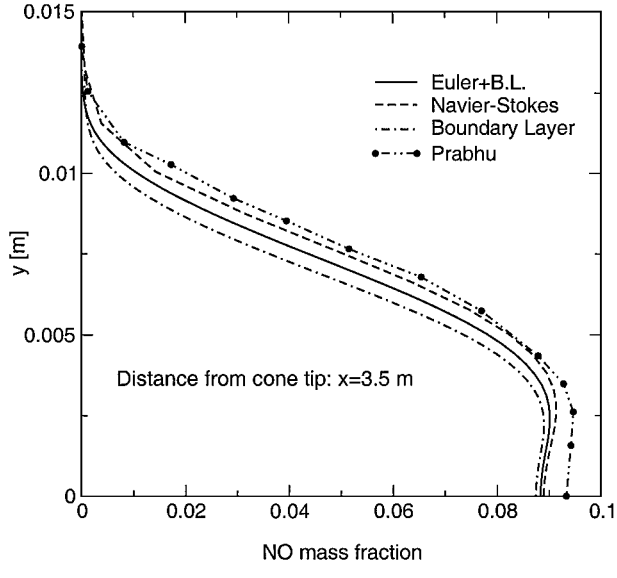

Fig. 14 NO mass fraction: comparison among different computations.

dynamic phenomena. This taken into account, the agreement between the computations is quite good. Except very close to the cone tip where viscous/inviscid interaction effects, which are neglected in the Euler/boundary-layer analysis, are important, the maximum difference is on the skin-friction coefficient, and it does not exceed 7% (Fig. 12; $x > 5$ cm) and, what is more important, the main physical features are equally captured by both approaches. We observe that both C_f and S_t are slightly overpredicted by Euler + boundary layer away from the problematic cone-tip region. This slight overprediction might be caused by the boundary-layer displacement effect in the Navier–Stokes in contrast to the Euler + boundary-layer approach.

Concerning the relative computational efficiency, the Euler + boundary-layer approach needed 28% of the CPU time needed by the full Navier–Stokes one. (All of the computations were performed on an AMD 500 MHz Athlon machine.) If we consider the good agreement between the two computations, we can conclude that, even nowadays, a Euler + boundary-layer approach, when physically sound, is more economical than a full Navier–Stokes one.

We would like now to compare more in detail the different computations on the cone, that is, the Euler + boundary-layer, the Navier–Stokes, the boundary layer, and the one of Ref. 24. In Figs. 13, 14, and 15 the nondimensional temperature, the nitric oxide NO mass fraction, and the atomic oxygen O mass fraction across the boundary layer at a distance $x = 3.5$ m from the cone tip are shown, respectively. The y coordinate on all of the three figures represents the physical transverse distance in the boundary layer. For the boundary-layer computation the physical thickness has been obtained from the transformed coordinate η by inverting Eq. (10). First, we notice that the boundary-layer thickness is indeed well predicted by both kinds of boundary-layer computations; this is a further indication of the validity of the Euler + boundary-layer approach for the specific circumstance. The temperature profiles (Fig. 13) are similar across the boundary layer, especially at the wall. The wall being noncatalytic, the only contribution to the heat flux comes from the conductive term $(-\lambda \nabla T)$, which is quite similar in all of the cases, and this explains the good agreement on the Stanton number. The profiles for NO and O are in good agreement, with the computation of Prabhu et al.[24] giving a stronger dissociation near the wall. In particular the NO behavior next to the wall (see Fig. 14) is really the same for our three computations, with only a negligible difference in the mass fraction value. This can be expected because the same physico-chemical models are used.

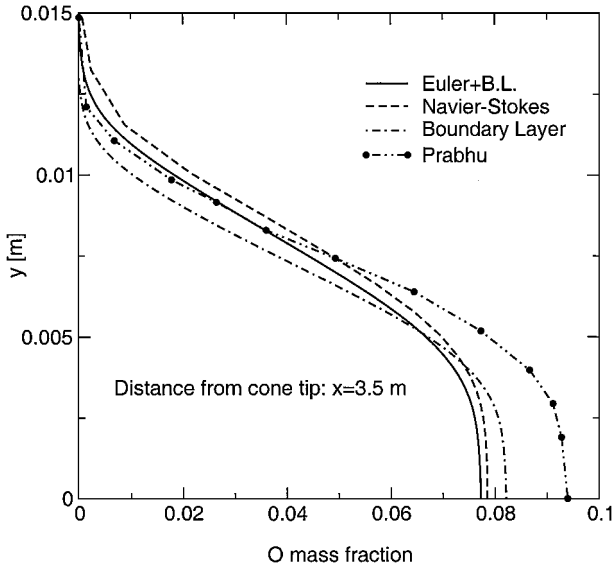

Fig. 15 O mass fraction: comparison among different computations.

Conclusions

A two-dimensional/axisymmetric boundary-layer code has been developed; efficient and accurate Hermitian-type multipoint finite difference schemes are used to discretize the governing equations. The code is able to handle arbitrary mixtures of perfect gases and utilizes up-to-date physico-chemical models for thermodynamic and transport properties and chemical kinetics. Diffusion fluxes are modeled by means of exact (in the framework of Chapman–Enskog theory) Stefan–Maxwell equations. Wall catalyticity is taken into account by means of a model that allows one to express a suitable set of wall reaction with their reaction rates.

The results of the computations show that the code is accurate, reliable, and able to handle a wide range of nonequilibrium conditions. In addition, when physically sound the boundary-layer code can be coupled with an Euler code to provide heat flux and skin friction at a fraction of the cost of a full Navier–Stokes computation.

In the highly complex hypersonic flight vehicle environment with a plethora of phenomenological and parametric inputs of uncertain accuracy or inadequate availability, the latter approach can serve as a handy design tool for quick estimates and parametric studies based on any given set of available models and input data. The said input data, it can be noted, are themselves active areas of physico-chemical research, and accordingly hypersonic researchers must be ready to continually update the needed inputs in order to improve the predictive capabilities of their CFD codes and their indispensable validation by increasingly sophisticated experiments that can resolve details from refined models.

Acknowledgments

The first author's research was supported by a Marie Curie Grant in the 4th Framework of the Training and Mobility of Researchers Program of the European Community. Partial support through INTAS Project 95-1329 (Coordinator: G. S. R. Sarma) is also appreciated. Thanks are accorded to the reviewers for perceptive remarks and suggestions that enabled us to improve our presentation and sharpen our observations.

References

[1]Sarma, G. S. R. (ed.), *Aerothermochemistry for Hypersonic Technology LS 1995-04*, von Kármán Inst., Rhode Saint Genèse, Belgium, 1995, pp. 1–44.

[2]Sarma, G. S. R., "Physico-Chemical Modeling for Hypersonic Flow Simulation," *Progress in Aerospace Sciences*, Vol. 36, Nos. 3–4, 2000, pp. 281–349.

[3]Kolesnikov, A. F., "Combined Measurements and Computations of High Enthalpy and Plasma Flows for Determination of TPM Surface Catalycity," *Measurement Techniques for High Temperature and Plasma Flows*, RTO-EN-8, NATO-RTO, Neuilly-Sur-Seine, France, 2000.

[4]Gupta, R. N., Yos, J. M., Thompson, R. A., and Lee, K. P., "A Review of Reaction Rates and Thermodynamic and Transport Properties for an 11-Species Air Model for Chemical and Thermal Nonequilibrium Calculations to 30000 K," NASA RP 1232, Aug. 1990.

[5]Park, C., "Problems of Rate Chemistry in the Flight Regimes of Aeroassisted Orbital Transfer Vehicles," *Thermal Design of Aeroassisted Orbital Transfer Vehicles*, edited by H. F. Nelson, Vol. 96, Progress in Aeronautics and Astronautics, AIAA, New York, 1985, pp. 395–418.

[6]Bottin, B., Vanden Abeele, D., Carbonaro, M., Degrez, G., and Sarma, G. S. R., "Thermodynamic and Transport Properties for Inductive Plasma Modeling," *Journal of Thermophysics and Heat Transfer*, Vol. 13, No. 3, 1999, pp. 343–350.

[7]Barbante, P. F., "Chemically Reacting High Temperature Gas Flow Around a Stagnation Point," von Kármán Inst., Diploma Project Rept. 1996-3, Rhode Saint Genèse, Belgium, June 1996.

[8]Wilke, C. R., "A Viscosity Equation for Gas Mixture," *Journal of Chemical Physics*, Vol. 18, No. 4, 1950, pp. 517–519.

[9]Mason, E. A., and Saxena, S. C., "Approximate Formulae for the Thermal Conductivity of Gas Mixture," *Physics of Fluids*, Vol. 1, No. 5, 1958, pp. 361–369.

[10]Sutton, K., and Gnoffo, P., "Multi-Component Diffusion with Application to Computational Aerothermodynamics," AIAA Paper 98-2575, June 1998.

[11]Barbante, P. F., "Accurate and Efficient Modelling of High Temperature Nonequilibrium Air Flows," Ph.D. Dissertation, von Kármán Inst.—Univ. Libre de Bruxelles, Brussels, May 2001.

[12]Hirschfelder, J., Curtiss, C., and Bird, R., *Molecular Theory of Gases and Liquids*, Wiley, New York, 1954, pp. 478–491.

[13]Ramshaw, J., and Chang, C., "Ambipolar Diffusion in Two-Temperature Multicomponent Plasmas," *Plasma Chemistry and Plasma Processing*, Vol. 13, No. 3, 1993, pp. 489–498.

[14]Scott, C. D., "Wall Catalytic Recombination and Boundary Conditions in Nonequilibrium Hypersonic Flows with Applications," *Advances in Hypersonics*, edited by J. J. Bertin, J. Periaux, and J. Balmann, Vol. 2, Birkhäuser, Cambridge, MA, 1992, pp. 176–250.

[15]Peters, N., "Lösung der Grenzschichtgleichungen für Chemisch Reagierende Gase mit Einem Mehrstellenverfahren," Deutsches Zentrum für Luft und Raumfahrt, FB-72-58, Göttingen, Germany, Aug. 1972.

[16]Straub, D., Schönauer, W., Schaber, A., Lin, S., and Adams, E., "Stationäre Laminare Hyperschallgrenzschichten um ein Rotationshy-Perboloid bei Thermochemischem Gleichgewicht der Luft," Deutsches Zentrum für Luft und Raumfahrt, FB-72-16, Göttingen, Germany, Feb. 1972.

[17]Lewis, C. H., "Non Reacting and Chemically Reacting Viscous Flows on a Hyperboloid at Hypersonic Condition," AG 147-70, AGARD, Sept. 1970.

[18]Fay, J. A., and Riddell, F. R., "Theory of Stagnation Point Heat Transfer in Dissociating Air," *Journal of Aeronautical Sciences*, Vol. 25, No. 2, 1958, pp. 73–85.

[19]Reggiani, S., Barbato, M., Bruno, C., and Muylaert, J., "Model for Heterogeneous Catalysis on Metal Surfaces with Applications to Hypersonic Flows," AIAA Paper 96-1902, June 1996.

[20]Bottin, B., Paris, S., Van Der Haegen, V., and Carbonaro, M., "Experimental and Computational Determination of the VKI Plasmatron Operating Envelope," AIAA Paper 99-3607, June–July 1999.

[21]de la Llave Plata, M., "Analysis and Application of a Methodology for the Determination of TPS Materials Catalycity," von Kármán Inst., Diploma Project Rept. 2000-4, Rhode Saint Genèse, Belgium, June 2000.

[22]Blottner, F., "Nonequilibrium Laminar Boundary Layer Flow of Ionized Air," *AIAA Journal*, Vol. 2, No. 11, 1964, pp. 1921–1927.

[23]Blottner, F., "Finite Difference Methods of Solution of the Boundary Layer Equations," *AIAA Journal*, Vol. 8, No. 2, 1970, pp. 193–205.

[24]Prabhu, D., Tannehill, J., and Marvin, J., "A New PNS Code for Chemical Nonequilibrium Flows," *AIAA Journal*, Vol. 26, No. 7, 1988, pp. 808–815.

[25]Barbante, P. F., and Degrez, G., "An Efficient Euler/Navier–Stokes Solver for Reacting Flows," 16th IMACS World Congress 2000, No. 411-3, Lausanne, Switzerland, Aug. 2000.